

This is the accepted manuscript made available via CHORUS. The article has been published as:

Topologically Protected Generation of Stable Wall Loops in Nematic Liquid Crystals

Tomohiro Ouchi (〇〇〇〇), Koki Imamura (〇〇〇〇), Kanta Sunami (〇〇〇〇), Hiroyuki Yoshida (〇〇〇〇), and Masanori Ozaki (〇〇〇〇)

Phys. Rev. Lett. **123**, 097801 — Published 29 August 2019

DOI: [10.1103/PhysRevLett.123.097801](https://doi.org/10.1103/PhysRevLett.123.097801)

Topologically-protected generation of stable wall loops in nematic liquid crystals

Tomohiro Ouchi (大内智弘),¹ Koki Imamura (今村弘毅),¹ Kanta Sunami (角南寛太),¹
Hiroyuki Yoshida (吉田浩之),^{1,2*} and Masanori Ozaki (尾崎雅則)¹

¹*Division of Electrical, Electronic and Information Engineering, Graduate School of
Engineering, Osaka University,
2-1 Yamada-oka, Suita, Osaka 565-0871, Japan*

²*Precursory Research for Embryonic Science and Technology (PRESTO), Japan Science
and Technology Agency (JST),
4-1-8 Honcho, Kawaguchi, Saitama 332-0012, Japan*

*) Author for Correspondence: E-mail: yoshida@eei.eng.osaka-u.ac.jp

Tel: +81-6-6879-7759, Fax: +81-6-6879-4838

Abstract:

The nematic liquid crystal (LC) director field can contain defects that are both singular and nonsingular, but nonsingular defects with an integer winding number of the director are typically metastable because of their high energy. Here, we demonstrate topology-mediated generation and stabilization of nonsingular wall loops in a sandwich-type LC cell by combining a patterned substrate with a planar substrate. We implement a design which imposes a topological constraint on a singular disclination loop such that it irreversibly annihilates upon application of a field, and results in the generation of a stable nonsingular wall loop when the field is removed. Theoretical modelling agrees with experimental observations, providing insight into the wall generation mechanism and its stability. The concept to stabilize high energy structures through orientation-patterning-defined topological constraints extends our ability to control orientationally ordered matter.

1 The nematic liquid crystal (LC) is a phase in which the constituent rod-like molecules
2 spontaneously orient along a single direction, referred to as the director. The nematic
3 director field can accommodate defects that are either singular or nonsingular,
4 characterized by the number of rotations of the director around the defect core [1, 2].
5 Singular defects can exist as lines or points, and have been studied from various
6 perspectives, from testing topological theorems [3, 4] to utilizing them to modulate the
7 local physical properties [5] or as templates for dopant materials [6-12].

8
9 In contrast to singular defects, nonsingular defects are much less explored. Nonsingular
10 defects occur as spatially localized excitations in the director field, and have continuous
11 structures that are topologically equivalent with a uniformly aligned nematic [2]. In a
12 sandwich-type nematic cell with planar boundary conditions, nonsingular defects appear
13 at the boundary of two topologically equivalent regions in the form of walls, with the
14 director locally orienting perpendicular to the substrates [13-17]. However, the steep
15 variation in the orientation makes them high energy such that wall loops formed at the
16 isotropic-nematic phase transition shrink and disappear over time [13]. Also, the property
17 of LCs to minimize their free energy creates a tendency for walls to split into lower energy
18 disclinations (singular line defects) [6]. Consequently, the study of walls had been mainly

1 limited to those that appear only under an external field [18], offering little freedom in
2 their control. While the growing interest in defects has led to various strategies for the
3 control of disclinations, such as the inclusion of colloidal particles [3-4,19] and use of
4 patterned substrates [6,20-22], little attention had been paid on actively controlling
5 nonsingular defects.

6
7 In this letter, we present a strategy to stabilize arbitrarily-shaped wall loops in an achiral
8 nematic LC through surface anchoring design of a sandwich-type cell. A combination of
9 a uniform planar and a suitably patterned substrate generates a looped disclination, which
10 upon application and cessation of an electric field, is converted into a stable wall loop.
11 The conversion makes use of the local incompatibility in director topology so that
12 regeneration of the singular disclination is suppressed although it has lower energy than
13 the wall. The wall position is well reproduced by theoretical modelling, clarifying the
14 underlying stabilization mechanism. Our approach enables selective stabilization of high
15 energy defect structures, extending our control over orientationally ordered matter.

16
17 Figure 1 depicts the easy axis distributions to stabilize a circular wall loop. The easy
18 axis on one substrate (“patterned substrate”) is patterned such that the azimuthal angle,

$\varphi_p(r)$, is given by Eq. (1) in cylindrical coordinates, where r is the position along the radius from the pattern center:

$$\varphi_p(r) = -\frac{\pi}{r_0}r + \frac{3\pi}{2}, \quad 0 \leq r \leq \frac{3r_0}{2}. \quad (1)$$

The azimuthal angle changes by π over a distance of r_0 , and extends to $3r_0/2$. Another substrate (“uniform substrate”) is prepared to possess uniform orientation, and a sandwich cell is fabricated using the two substrates so that the easy axis of the uniform substrate is parallel to the region of 0 radian on the patterned substrate.

A $\sim 8 \mu\text{m}$ -thick sandwich cell was prepared using two substrates coated with polyimide (JSR, AL1254) and photoalignment agent (DIC, LIA-03). The substrate with polyimide was rubbed unidirectionally, whereas the substrate with the photoalignment layer was patterned to possess the easy axis distribution of Fig. 1(a) using maskless photoalignment [22]. The photoalignment setup imprinted the local orientational easy axis over an area of $1,024 \times 768$ pixels, where each pixel size was $\sim 1.3 \times 1.3 \mu\text{m}^2$. The pattern was digitized to 3° steps and imprinted with a light dosage of $0.3 \mu\text{J}/\text{pixel}$. After cell fabrication, a nematic LC (5CB, Merck) was injected into the cell in the isotropic phase, and observed at 30°C using a polarizing optical microscope (POM, Nikon, LV100 POL).

Figure 2 (a) shows a schematic of the LC-filled cell. A nematic LC confined between two substrates with different easy axis directions twists in the bulk to minimize the elastic free energy [1]. Because 5CB is achiral, the director twists in the direction that reduces the twist angle. The twist angle distribution expected from the pair of substrates used is shown in Fig. 2(c), where the twist angle is kept below $|\pi/2|$ in all regions. At $r = r_0$, the twist angle changes discontinuously by π , and changes the twist direction from left ($r < r_0$) to right ($r > r_0$). The π jump in twist angle is accompanied by a singular disclination, and appears as a black line floating in the LC.

Figure 2(d-f) shows POM images of the sample with $r_0 = 107 \mu\text{m}$. Between crossed polarizers, light is transmitted where its polarization changes due to director twisting. The disclination loop appears as a thin dark line at approximately $r = r_0$, and is also observed without the analyzer. Insertion of a first order retardation plate ($\lambda = 530 \text{ nm}$) shows that the twist sense is inverted at the defect, but there is no tilt induced in the director, since no significant change in birefringence occurs near the disclination.

Generally, disclinations possess a line tension and tend to shrink [1,24]. However, the easy axis on the patterned substrate is designed such that the elastic energy due to director

distortion increases with disclination shrinkage. That is, because the twist angle can only change discontinuously at the disclination, its displacement from position r_0 to $(r_0 - \Delta r)$ causes the twist inversion to occur at twist angles of $(\pi\Delta r/r_0 \mp \pi/2)$ instead of $\mp\pi/2$. This increases the twist component of the elastic energy, which is proportional to the square of the twist rate [1]. The disclination loop is stabilized where the free energy of the disclination relieved by shrinkage is balanced by the increase in the elastic energy [22] (see also SI Section 1).

After confirming the generation of a disclination loop, an electric field (1 kHz, 2.5 V) was applied between the substrates. The electric field reorients the director perpendicular to the substrates and untwists the director [1], causing the disclination to shrink and annihilate over time. When the field is removed after disclination annihilation, the disclination does not reappear, but a nonsingular wall loop is generated at $r \sim 1/2r_0$ (Fig. 2(h-j) and Supplementary Movie 1). The wall loop is stable and only disappears when the sample is heated into the isotropic phase, but upon reentering the nematic phase, the disclination reappears, implying that the configuration with the disclination has lower energy. The wall appears thicker than the disclination and can also be observed without the analyzer. Insertion of the retardation plate reveals a color change in regions separated

1 by the wall, implying again a large change in twist angle at the wall. On the other hand,
2 the color changes inside the wall, implying that now there is an out-of-plane tilt
3 deformation of the director.

4
5 The above observations allow us to interpret the disclination-to-wall transition
6 mechanism as follows. Consider a cross-sectional area of the cell containing a section of
7 the disclination that runs perpendicular to the plane (Fig. 2(a)). The topological properties
8 of a line defect can be analyzed by taking a circular path around the disclination core and
9 mapping the orientation along the path on a sphere representing all the possible
10 orientation directions (i.e., order parameter space) [2]. Defects in LCs are also commonly
11 characterized by their strength: it is the number of 2π rotations of the director along a
12 circular path that surrounds the defect, and can take half-integers or integers. In a three-
13 dimensional nematic, defects with half-integer strength can be continuously transformed
14 into a defect of strength $1/2$, and those with integer strength can be transformed into a
15 uniformly aligned state with strength 0. Thus, the topological invariant, or charge, can
16 only take two values, either $1/2$ or 0 (in terms of defect strength), and must be conserved
17 according to the following: $1/2 + 0 = 1/2$ and $1/2 + 1/2 = 0$.

In Fig. 2(a), the disclination gives a contour on the order parameter space terminating at diametrically opposite points; it is a topologically stable singularity with charge $1/2$. Because there is another defect with opposite strength on the other side of the loop (at $\theta = \pi$), shrinkage of the defect by the applied field causes the disclination to eventually annihilate and give a net defect strength of 0. When the field is removed, the most stable configuration would be to have the two disclinations repositioned at their initial positions (recall that this configuration is always obtained through thermal phase transition). However, because the director is now everywhere continuous and free of singularities, there is locally a topological incompatibility that prohibits the regeneration of disclinations. Instead of returning to a state with two defects of charge $1/2$, the system is required to relax into a state with charge 0 everywhere, i.e., with 0 or integer defect strength.

Since shrinkage of the disclination loop causes the right-handed twist region (originally at $r > r_0$) to extend to below r_0 , a configuration with strength 0 corresponds to one that is right-handed everywhere. On the other hand, the configuration with strength 1 corresponds to one that accommodates a wall with a 2π jump in twist angle [23,24]. A completely right-handed configuration would require the maximum twist angle to reach

$3\pi/2$ at $r = 0$ whereas, while the wall has high energy density and its energy is proportional to its length, the maximum twist angle can be reduced to $\sim|\pi|$, if it is accommodated at $r = r_0/2$, where the easy axes on the substrates are parallel [Fig. 2(g)]. Thus, there is a competition between wall shrinkage and minimization of director twist acting in opposite directions, similar to the case of the disclination. Stabilization of the wall occurs as a result of the LC relaxing into a topologically-allowed configuration with lowest energy.

We analyze the free energy landscape of the director configuration with a wall loop and show that there is indeed an equilibrium loop radius that minimizes the energy. We base our analysis on a model for the wall proposed by Turner [15], which describes the director distribution using an analytical function with no singularities (SI Section 2). The Turner distribution has been found to be a close approximation to that obtained by minimizing the free energy numerically [17]. A cylindrical coordinate system is employed, with the uniform and patterned substrates placed at $z = -d/2$ and $d/2$, where d is the cell gap. A LC with splay, twist, and bend elastic constants of K_{11} , K_{22} , and K_{33} fills the cell and accommodates a circular wall loop with center at the origin and radius r_w .

To satisfy the boundary conditions set by orientation patterning, we modify the Turner

1 distribution and use the following, $\mathbf{n}_w(r, z)$, for a wall positioned at $r = r_w$:

$$\begin{aligned}
n_{w,x} &= \cos \left\{ \pi \cdot \left[1 + \left(-\frac{r}{r_0} + \frac{1}{2} \right) \cdot \tanh \{ m(r - r_w) \} \right] \cdot \left(\frac{z}{d} + \frac{1}{2} \right) \right\} \\
n_{w,y} &= \sin \left\{ \pi \cdot \left[1 + \left(-\frac{r}{r_0} + \frac{1}{2} \right) \cdot \tanh \{ m(r - r_w) \} \right] \cdot \left(\frac{z}{d} + \frac{1}{2} \right) \right\} \cdot \tanh \{ m(r - r_w) \} \quad (2) \\
n_{w,z} &= \sin \left\{ \pi \cdot \left[1 + \left(-\frac{r}{r_0} + \frac{1}{2} \right) \cdot \tanh \{ m(r - r_w) \} \right] \cdot \left(\frac{z}{d} + \frac{1}{2} \right) \right\} \cdot \operatorname{sech} \{ m(r - r_w) \}
\end{aligned}$$

3 The director changes its twist direction at $r = r_w$ as well as orients perpendicular to the
4 substrates, with a wall thickness defined by the parameter m (SI Section 3). Here we use
5 the following for m , which minimizes the free energy for a parallel planar boundary
6 condition [16]:

$$m = \frac{\pi}{d} \sqrt{\frac{K_{11} + K_{33} - 2K_{22}}{3K_{22} + K_{33}}} \quad (3)$$

8 In SI Section 4, we evaluate the topological charge of the wall in a single r - z plane using
9 Eq. (2), and show that it is indeed different from the disclination.

10

11 We numerically calculate the Oseen-Frank free energy of LCs, F , using \mathbf{n}_w (SI Section 5)
12 [1]. Figure 3 (a) plots F as a function of r_w , where $d = 7.95 \mu\text{m}$, and $r_0 = 107.2 \mu\text{m}$ as in
13 experiment, and $K_{11} = 4.85 \text{ pN}$, $K_{22} = 3.1 \text{ pN}$, $K_{33} = 6.1 \text{ pN}$ for 5CB [25]. F has a local
14 minimum at $r_w = 48.7 \mu\text{m}$, which agrees with the experimental equilibrium radius at 49
15 μm . Note that the proposed mechanism yields an equilibrium radius that is always smaller

1 than $r_0/2$, where intuitively, the wall is likely to appear. In fact, Supplementary Video 1
2 shows a two-step transition for wall generation and stabilization, where the wall first
3 appears at $r_0/2$ and then shrinks to the equilibrium position.

4
5 The validity of the model was investigated further by varying r_0 from 26.8 – 134 μm .
6 Figure 3 (b) compares the experimentally measured and theoretically predicted wall radii
7 (POM images shown in SI Section 6). For $r_0 > 50 \mu\text{m}$, experiment agrees well with theory,
8 with the deviation between the two falling within 3%. For $r_0 = 40.2 \mu\text{m}$, the wall had an
9 equilibrium radius of 15.2 μm , whereas theory predicted equilibrium at $r = 0$, i.e., the
10 director configuration without the wall to have lower energy. While this discrepancy is
11 believed to be a result of \mathbf{n}_w not fulfilling the Euler-Lagrange equations, we note that the
12 energy difference between director configurations with and without the wall approaches
13 0 at the crossover of the stable state, which makes both configurations equally stable and
14 thus prone to small fluctuations. Overall, the model reproduces the phenomenon more
15 than satisfactorily, validating the stabilization mechanism.

16
17 We also investigate the effect of varying r_0 and d on the wall stability. Fig. 3(c) shows
18 relative stabilities of the director configuration with the wall to that without, where the

1 dashed line represents the crossover condition of the stable configuration. Clearly,
2 increasing stability is predicted for larger r_0 and smaller d , which can be attributed to the
3 fact that the wall has to move over a greater area for larger r_0 , and, the director twist rate,
4 and hence the elastic energy penalty upon wall shrinkage, increases for smaller d . The
5 results also allow us to infer that a steep change in twist angle near the wall stabilizes it,
6 since the energy rises quickly even for small shrinkage.

7
8 Finally, we extend our strategy to stabilize an arbitrarily-shaped wall loop. Figure 4
9 shows disclination and wall loops stabilized in the shape of our school logo. The wall
10 appears approximately where the substrates have parallel orientation, and its stability
11 increases with a steeper change in twist angle. Following this principle, we create four
12 regions in the shape of the logo and obtain the easy axis distribution in each domain as
13 numerical solutions to Laplace's equation. For domains labelled I, II, and III in the figure,
14 the outer and inner boundary conditions are set to $(0, -\pi/2)$, $(\pi/2, 0)$, and $(0, 4\pi/9)$. The
15 sample first shows a disclination loop approximately at the boundary of domains I and II.
16 Upon applying and removing an electric field, the disclination annihilates and a wall loop
17 appears approximately at the boundary of domains II and III [Fig. 4(c,d), see also SI
18 section 7]. This demonstrates the versatility of our approach, allowing meaningful

1 symbols to be represented by stable walls.

2
3 In conclusion, we demonstrated a topology-mediated pathway for the generation of
4 high-energy, nonsingular wall loops in a nematic LC. The study is distinct from other
5 works in that a pure nematic LC with no inclusions is used in a planar cell structure, and
6 the generated loop, which can be designed arbitrarily, is stable without a sustaining
7 electric field. Other than motivating the search for designs to stabilize even higher energy
8 defects, our work opens doors to detailed investigations of defect structure and dynamics
9 [27], as well as its interaction with various dopants. Surface patterning allows positioning
10 of the defect, which is usually not possible with colloid-induced defects, and thus is
11 advantageous for potential applications of defects. Considering that steep changes in the
12 director not only affects the elastic energy of the system, but also the dielectric and
13 rheological properties, we anticipate the emergence of novel phenomena and applications
14 through the investigation of defect-matter interactions in a controlled environment.

15 16 **Acknowledgements**

17 This work was supported by JST PRESTO (JPMJPR151D) and JSPS KAKENHI
18 (17H02766). The authors thank DIC Corporation for providing the photoalignment

1 material and JSR Corporation for providing the planar alignment material.

2

3

- 1 [1] P. G. de Gennes and J. Prost, *Physics of Liquid Crystals* (Oxford University Press,
- 2 1993).
- 3 [2] K. Maucci, and O. D. Lavrentovich, *Soft Matter Physics: An Introduction*, (Springer-
- 4 Verlag, New York, 2003)
- 5 [3] B. Senyuk, Q. Liu, S. He, R. D. Kamien, R. B. Kusner, T. C. Lubensky, and I. I.
- 6 Smalyukh, *Nature* **493**, 200 (2013).
- 7 [4] S. Coper, and S. Žumer, *Phys. Rev. Lett.*, **106**, 177801 (2011).
- 8 [5] M. Zapotocky, L. Ramos, P. Poulin, T. C. Lubensky, and D. A. Weitz, *Science* **283**,
- 9 209 (1999).
- 10 [6] H. Yoshida, K. Asakura, J. Fukuda, and M. Ozaki, *Nat. Commun.* **6**, 7180 (2015).
- 11 [7] B. Senyuk, J. S. Evans, P. J. Ackerman, T. Lee, P. Manna, L. Vigderman, E. R.
- 12 Zubarev, J. van de Lagemaat, and I. I. Smalyukh, *Nano Lett.* **12**, 955 (2012).
- 13 [8] J. B. Fleury, D. Pires, and Y. Galerne, *Phys. Rev. Lett.* **103**, 267801 (2009).
- 14 [9] X. Wang, D. S. Miller, E. Bukusoglu, J. J. de Pablo, and N. L. Abbott, *Nat. Mater.* **15**,
- 15 106 (2016).
- 16 [10] X. Wang, Y. K. Kim, E. Bukusoglu, B. Zhang, D. S. Miller, and N. L. Abbott, *Phys.*
- 17 *Rev. Lett.* **116**, 147801 (2016).
- 18 [11] T. Ohzono, K. Katoh, and J. Fukuda, *Sci. Rep.* **6**, 36477 (2016).

- 1 [12]K. Kawaguchi, R. Kageyama, and M. Sano, Nature 545, 327-331 (2017).
- 2 [13]J. Nehring, Phys. Rev. A **7**, 1737 (1973).
- 3 [14]R. B. Meyer, Philos. Mag. **27**, 405 (1973).
- 4 [15]R. Turner, Philos. Mag. **30**, 13 (1974).
- 5 [16]R. Turner, Phys. Lett. A, **49**, 423 (1974).
- 6 [17]R. Turner, Philos. Mag. **31**, 719-722 (1975).
- 7 [18]A. d. Lózar, W. Schöpf, I. Rehberg, D. Svenšek, and L. Kramer, Phys. Rev. E **72**,
- 8 51713 (2005).
- 9 [19]U. Tkalec, M. Ravnik, S. Copar, S. Zumer, and I. Musevic, Science **333**, 62 (2011).
- 10 [20]M. Cavallaro, M. A. Gharbi, D. A. Beller, S. Čopar, Z. Shi, T. Baumgart, and K. J.
- 11 Stebe, Proc. Nat. Acad. Sci. **110**, 18804 (2013).
- 12 [21]M. Wang, Y. Li, and H. Yokoyama, Nat. Commun. **8**, 388 (2017).
- 13 [22]K. Sunami, K. Imamura, T. Ouchi, H. Yoshida, and M. Ozaki, Phys. Rev. E **97**,
- 14 020701 (2018).
- 15 [23]D. W. Berreman and W. R. Heffner, Appl. Phys. Lett. **37**, 109 (1980).
- 16 [24]C. Jones, *Handbook of Liquid Crystals*, 8nd ed. (Wiley-VCH Verlag Gmbh & Co.
- 17 KGaA, Weinheim, 2014), Chap. 4.
- 18 [25]I. W. Stewart, and R. J. Atkin, Physical Properties of Liquid Crystals: Nematics,

- 1 (INSPEC, 2001), Chap. 5.
- 2 [26] M. Ambrožič, S. Kralj, and E. G. Virga, Phys. Rev. E 75, 031708 (2007).
- 3

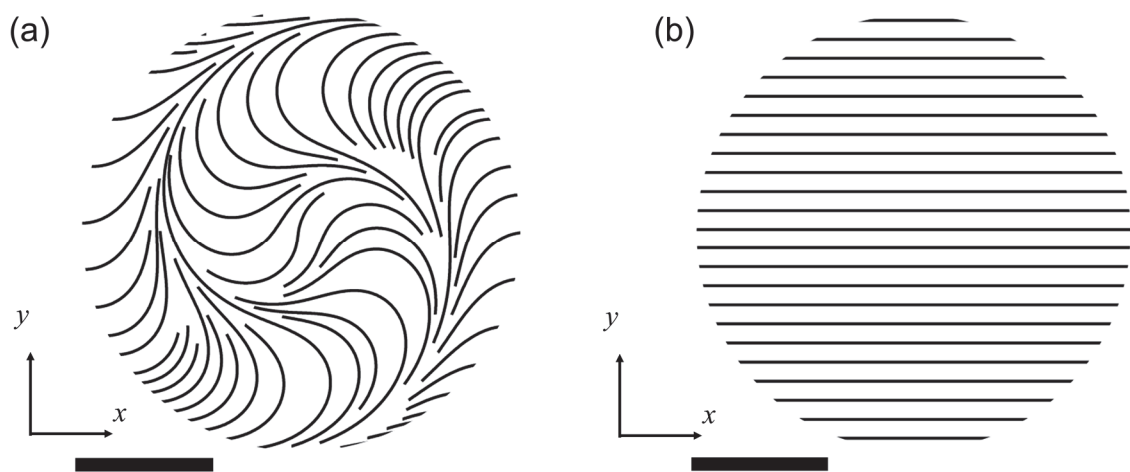


FIG. 1. (a) Streamline representations of the orientational easy axis on the patterned and (b) uniform substrates. Scale bars: 100 μm .

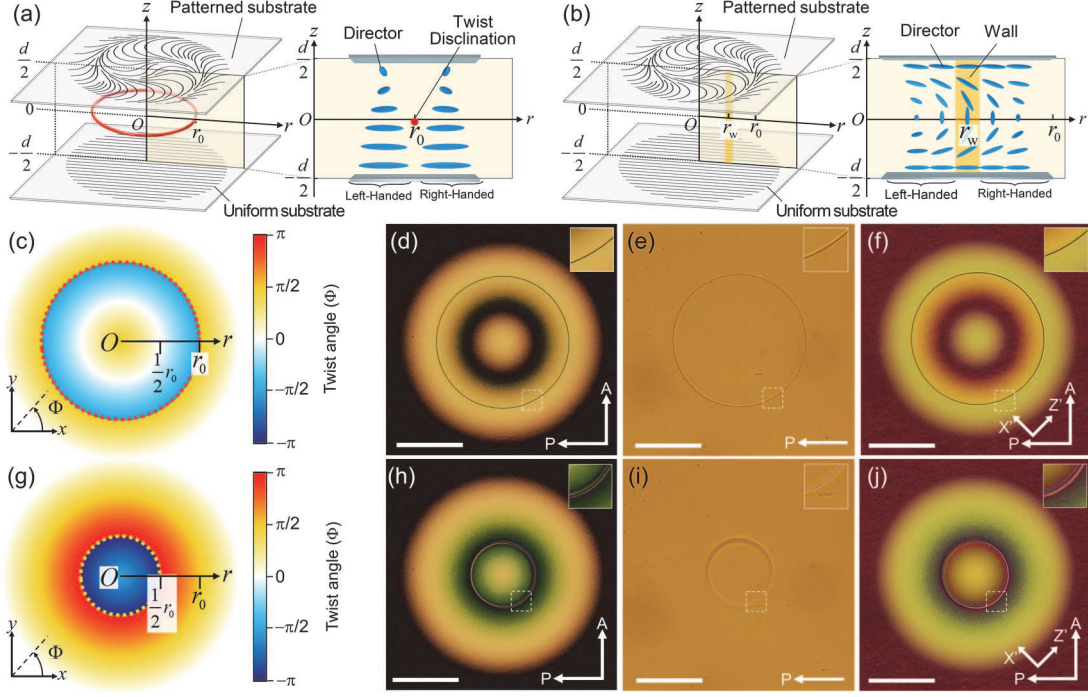
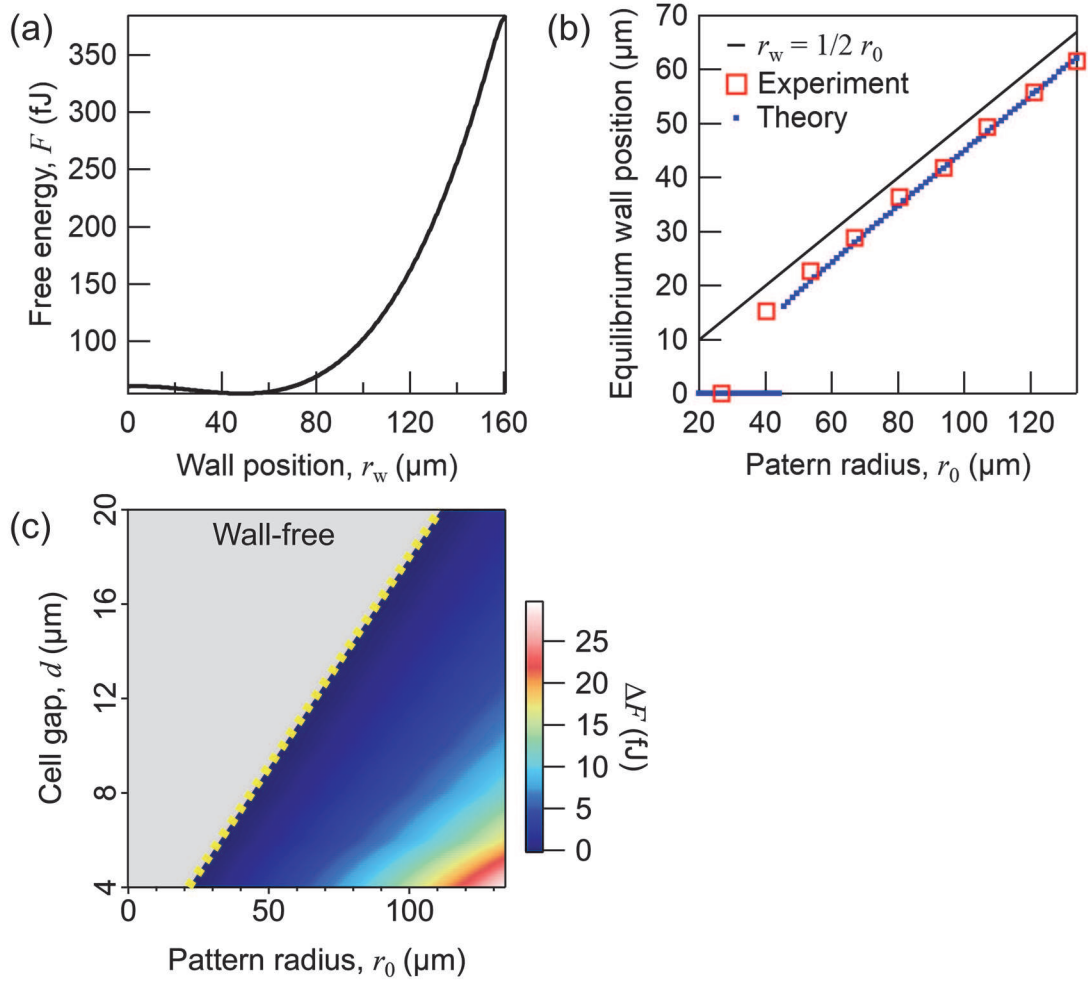
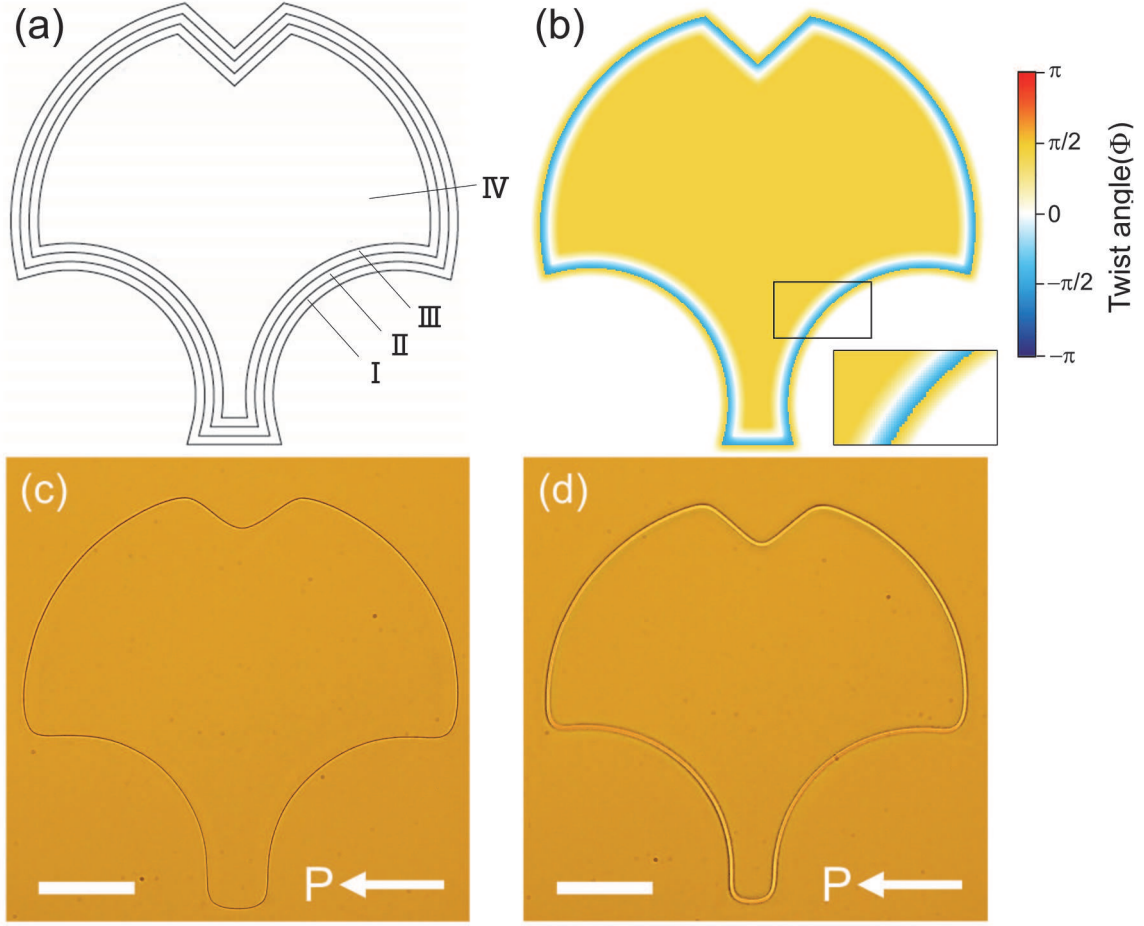


FIG. 2. (a) Schematic of LC cell with a disclination loop, and (b) wall loop. (c) Twist angle distribution between the substrates when a disclination is present. (d) Microscope images of the disclination loop between crossed polarizers, (e) without polarizer, and (f) with a 530 nm retardation plate, where X' and Z' are the fast and slow axes. (g) Twist angle distribution between the substrates when a wall is present. (h) Microscope images after wall generation between crossed polarizers, (i) without analyzer, and (j) with a retardation plate. Scale bars: 100 μm .



1
2 FIG. 3. (a) F versus r_w for a cell with $d = 7.85$ μm and $r_0 = 107.2$ μm. (c) Experimental
3 and theoretical equilibrium wall positions versus r_0 . Solid line indicates the ideal position
4 of wall with no shrinkage. (d) Stability of the director configuration with the wall loop
5 relative to the wall-free state for different cell parameters. Dashed line indicates the
6 crossover between the two configurations.

7



1
2 FIG. 4. (a) Osaka University logo divided into four areas. (b) Twist angle distribution to
3 generate the wall loop. (c) Optical microscope image of disclination loop and (d) wall
4 loop. Scale bars: 100 μm .